

# Electronic State Chromatography of Lutetium Cations

Biswajit Jana\*,<sup>1,2</sup> EunKang Kim,<sup>1,2</sup> Aayush Arya,<sup>1,2</sup> Elisa Romero Romero,<sup>1,2</sup> Elisabeth Rickert,<sup>1,2</sup> Harry Ramanantoanina,<sup>1,2</sup> Sebastian Raeder,<sup>2,3</sup> Michael Block,<sup>1,2,3</sup> and Mustapha Laatiaoui\*<sup>1,2,3</sup>

<sup>1</sup> *Department Chemie, Johannes Gutenberg-Universität, Fritz-Strassmann Weg 2, 55128 Mainz, Germany*

<sup>2</sup> *Helmholtz-Institut Mainz, Staudingerweg 18, 55128 Mainz, Germany*

<sup>3</sup> *GSI Helmholtzzentrum für Schwerionenforschung, Planckstrasse 1, 64291 Darmstadt, Germany*

(Dated: July 16, 2024)

Relativistic effects strongly influence the electronic structures of the heaviest elements, thereby shaping their chemical and physical properties. Studying ion mobility within a noble gas environment reveals how the ion-neutral interactions depend on the ion's electronic configurations, thus providing an avenue for exploring these effects. An ion mobility spectrometer with a cryogenic drift tube was developed to precisely measure the low-field reduced mobility of heavy lanthanide and actinide cations. The apparatus was characterized by optimizing the bunching operation of ions with a miniature RF coulomb buncher and evaluating the chromatography performance of the drift tube operated with helium buffer gas at a temperature of 298K. Systematic ion mobility measurements of lutetium cations ( $\text{Lu}^+$ ) drifting in helium gas were carried out as a case study. The electronic state chromatography of  $\text{Lu}^+$  has been demonstrated. The low-field reduced ion mobility for the ground and lowest meta-stable state of  $\text{Lu}^+$  have been examined. In addition, the variation of both states' reduced mobility and the quenching of meta-stable population has been investigated under different reduced electric fields ( $E/n_0$ ), the ratio of an electric field to neutral gas number density.

Keywords: Ion transport, Ion mobility spectrometry, electronic state chromatography, low-field reduced ion mobility.

## I. INTRODUCTION

Heavy elements in the periodic table exhibit different chemical and physical properties [1],[2] due to their unique electronic structures, strongly influenced by relativistic effects [3],[4]. As the atomic number ( $Z$ ) increases, the velocity of inner shell electrons orbiting the nucleus also increases. To conserve the angular momentum, it results in a contraction of inner  $s$  and  $p$  orbitals towards the nucleus[5]. This contraction effectively shields the nuclear potential, impacting various properties such as electrons' binding energy, valence electron configuration, inter-atomic forces, bond lengths, and enthalpies. Consequently, these factors collectively shape the chemical behaviour of the heavy elements. So, the relativistic effects play a crucial role in determining the behaviour of heavy atomic systems, particularly within the lanthanide and actinide series[6]. These elements exhibit distinct chemical and physical characteristics that deviate significantly from traditional chemical trends. Understanding the intricate relationship between relativistic effects and electronic structures [7] is essential for unravelling the unique properties of heavy elements. It also provides a distinctive avenue for predicting and exploring the electronic structures of super heavy elements, which do not exist on earth but can be synthesized only on a one-atom-at-a-time scale.

Ion Mobility Spectrometry (IMS)[8],[9] is a powerful analytical technique in structural analysis, offering valuable insights into the composition, conformation, and interactions of ions within a dilute buffer gas. At its core, ion mobility measures an ion's drift velocity ( $v_d$ ) travelling through a buffer gas under a uniform electric field ( $E$ ). The drift velocity is expressed as[8] :

$$v_d = K \cdot E \quad (1)$$

where  $K$  is the mobility constant. Generally, the mobility is reported as reduced mobility ( $K_0$ ), which is the ion mobility at standard pressure ( $P_0$ ) and temperature ( $T_0$ ) according to [8].

$$K_0 = K \left( \frac{P}{P_0} \right) \left( \frac{T_0}{T} \right) \quad (2)$$

where  $P$  and  $T$  are the buffer gas pressure and temperature. From kinetic theory, the reduced mobility is given by Mason-Schamp equation [10, 11] :

$$K_0 = \left( \frac{3Ze}{16n_0} \right) \sqrt{\frac{2\pi}{\mu k_B T_{eff}}} \frac{1}{\Omega} \quad (3)$$

where  $e$  is the electron charge,  $k_B$  is the Boltzmann constant,  $\mu$  is the ion's reduced mass,  $n_0$  is the gas number density,  $T_{eff}$  is the effective temperature of ions and  $\Omega$  is the ion-neutral collision cross-section. The reduced mobility is thus sensitive to the collision cross-section, which depends on the ion-neutral interaction potential. This potential [12] depends on the long-range ion-induced dipole attraction, its higher-order interaction, and short-range repulsion. From these interdependencies, one can

\*Corresponding author: bjana@uni-mainz.de

\*Corresponding author: mlaatiaoui@uni-mainz.de

ultimately conclude that IMS is sensitive to an element's electronic configuration and polarizability [13, 14] via the ion-neutral interaction potentials. From a theoretical perspective [11], it is possible to calculate transport properties like mobility and diffusion coefficients, collision integrals, and momentum transfer cross-sections with relatively high accuracy from the knowledge of the ion-atom interaction potential. Such a potential can be assessed in the transport calculations, making ion mobility data valuable for benchmarking both transport and relativistic *ab initio* calculations [15].

Ion mobility studies on lighter elements have revealed mobility deviations when the electronic configurations change drastically. For instance, an extra  $d$  electron in the ground-state configuration of gadolinium leads to an 11% deviation in ion mobilities between  $\text{Eu}^+$  and  $\text{Gd}^+$  [16]. The metastable ionic states have also been identified from the ground states [9, 17]. For instance,  $\text{Cu}^+$  ions in the configurations  $[\text{Ar}]3d^{10}$  and  $[\text{Ar}]3d^94s^1$  drifting in helium gas show a deviation of about 33%, caused by the  $s$  orbital occupation in the metastable state [18]. These findings emphasize how ion-atom interaction potentials and ion mobilities are sensitive to electronic configurations, paving the way for electronic-state chromatography and state-selected ion chemistry [9] as well as Laser Resonance Chromatography [19] towards studying the heaviest elements' electronic structure.

This article describes a cryogenic drift tube-based ion mobility spectrometer developed for the study of heavy elements, particularly lanthanides and actinides. The experimental setup is briefly reported in section II. Section III presents the chromatography performance of the setup's medium-sized cryogenic drift tube as well as results from systematic ion mobility measurements on  $\text{Lu}^+$  as a case study. Section IV concludes with a short summary and outlook.

## II. EXPERIMENTAL SETUP

Fig. 1 illustrates the schematic of the developed ion mobility spectrometer setup. It consists of three distinct pressure sections (PS) interconnected through diaphragms with an opening diameter of 3 mm. Each pressure section is connected to individual turbo-molecular pumps (TMP). A dry pump (Edwards iXL600) with a pumping speed of  $600 \text{ m}^3/\text{hr}$  serves as a backing pump for the turbo-molecular pumps.

The first pressure section (PS1) incorporates key subsystems such as a laser ablation (ion) source, a miniature RF ion buncher, a cryogenic drift tube, and a miniature RF ion guide. This section is evacuated by a TMP (Edwards STPA-1603C) with a maximum pumping speed of  $1250 \text{ l/s}$  for helium gas. The pump has a variable speed feature, adjustable from 18 to 36 krpm. The typical targeted vacuum level in PS1 is approximately  $10^{-2} \text{ mbar}$

for efficiently catching and bunching ions.

On the other hand, PS3 houses a quadrupole mass spectrometer followed by a channeltron detector, requiring a vacuum of approximately  $10^{-6} \text{ mbar}$ . A TMP (Leybold TURBOVAC 361) evacuates this section. To bridge the vacuum levels between these two sections, i.e. PS1 and PS3, an intermediate pressure section, PS2 is incorporated. The PS2 contains an RF ion guide for efficiently guiding and transporting the ion bunch from PS1 to PS3. The PS2 section is evacuated by another TMP (Edwards STP 451), which enables it to achieve a vacuum level of  $10^{-4} \text{ mbar}$ .

Helium buffer gas is injected with controlled flow rates into the drift tube and PS1 through two independent needle valves. These valves are connected to a common gas line linked to a helium gas bottle through a gas purifier with a gas getter (type: Mono-Torr, PS4-MT3-R-2). Helium gas with a purity of at least 99.996% is used during experiments. The pressure inside the drift tube is measured by a calibrated capacitance gauge (type: Pfeiffer CMR 261), while the vacuum levels in different sections are measured using a combined Pirani and cold cathode gauge (type: Pfeiffer, PKR 251). The vacuum levels in the different pressure sections and in the drift tube were measured with the He gas flow into the drift tube, and it was observed that the setup could be safely operated at a drift-tube pressure of 10 mbar. The different components of the experimental setup are discussed below.

### A. Ion source

The ion source is made of a copper plate, with its front surface at a 45-degree angle to the centre axis of the apparatus. A thin foil (0.025 to 0.1 mm thickness) of the desired element, such as lutetium (Lu), is affixed to the front surface of the copper plate using a silver adhesive (Silver DAG 1415). This source is axially inserted to face a view-port for the ablation laser beam and is positioned at an axial distance of 20 mm from the entrance of the miniature RF coulomb buncher structure. A 1 mm thin stainless steel plate with a diameter of 70 mm, referred to as a shielding plate, is attached to the source from the back side for improved ion focusing towards the ion buncher. An Nd:YAG laser (type: Continuum, Precision II) is employed for the ablation process, operating at a repetition rate of 50 Hz and a wavelength of 355 nm. The experiment control and data acquisition system (DAQ) externally triggers the laser. A 500 mm focal length lens is positioned in front of the chamber viewport to focus the laser beam onto the target. The position of the laser beam on the target foil is user-controlled using a piezo-driven mirror (type: KIM101, Thorlab). During experiments, the laser beam is spatially scanned over the source around the targeted spot to prevent the focused beam from creating craters or holes. Multiple foils can

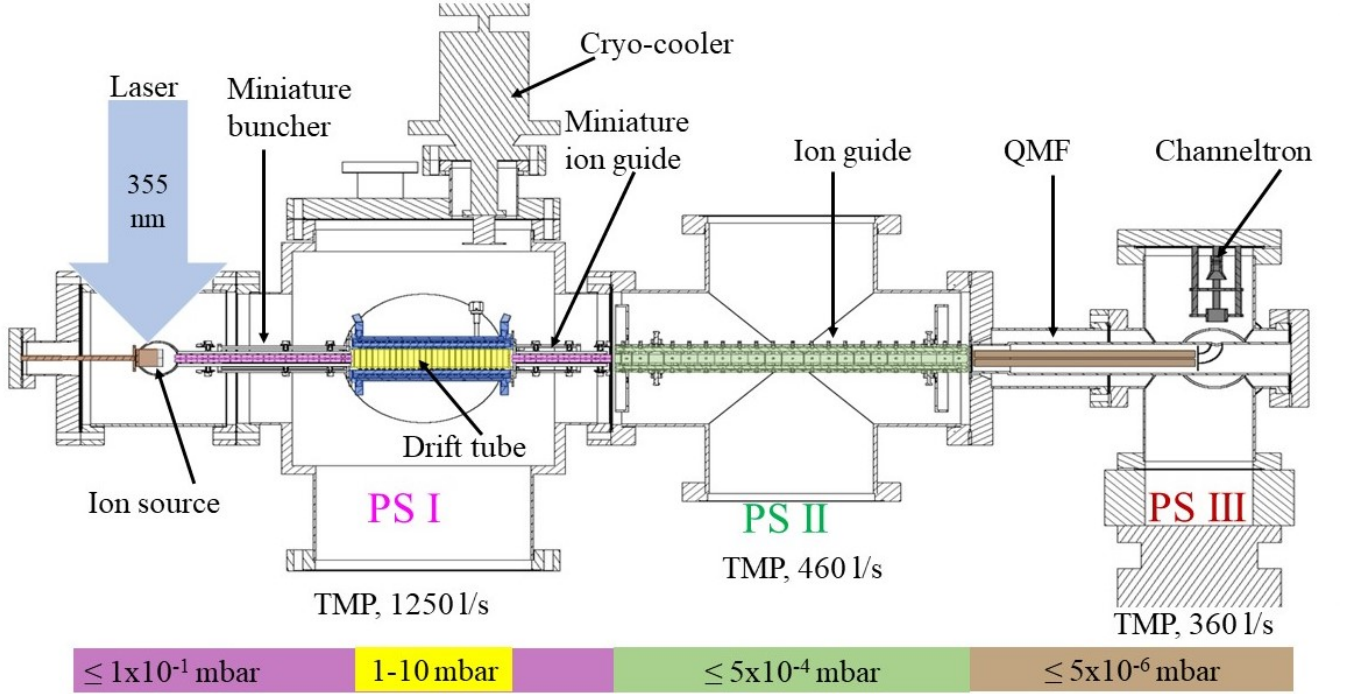


FIG. 1: Schematic overview of the developed ion mobility spectrometer. Typical pressure ranges are indicated for each pumping section of the apparatus.

be installed at the same time, and the laser beam spot can be quickly shifted to different foils of the different elements based on needs (without breaking the vacuum). Although the laser has very high power, we utilise a minimal power range, typically between 2 mW to 20 mW, for the ablation of lanthanide elements. It has also been observed that the plasma density of laser ablated plume is higher at higher power levels, resulting in fewer ions being collected by the ion buncher than at lower power levels.

### B. Miniature ion buncher and ion guide

The ion buncher and ion guide work on the principle of linear Paul trap [20, 21]. Here, a miniature ion buncher and miniature ion guide were developed. The miniature ion buncher is approximately 166 mm long and has 17 segments. Each segment has four rods with a diameter of 3.5 mm arranged in a quadrupole configuration, with a 3 mm distance between opposite rods. The spacing between segments ranges from 0.2 to 0.5 mm. The standard segment length is 10 mm long. The last segment (S17) is 8 mm long, and the second-to-last segment (S16) is 3 mm.

The design of the miniature ion guide is similar to that of the miniature ion buncher. It has a length of 94 mm and 9 segmented electrodes, each 10 mm long. Applying

RF voltages with mirrored phases to neighbouring rods creates a harmonic pseudopotential between the rods. This confines the ions radially around the centre axis of the RF structure. In the ion buncher, the ions pass through various stages. Firstly, they are captured and radially confined by the RF potentials. Then, the ions are axially transported by a DC gradient from its entrance to the potential well formed at buncher segment number 16 (S16), which is close to the drift tube entrance orifice. In the potential well, the ions are cooled down and trapped for a predefined time before the ion bunch is injected into the drift tube. The detailed description of the bunching process in a similar setup is described elsewhere [22].

The DC potentials on segments S1 to S14 are applied through a linear resistor chain. Two fast high-voltage transistor switches (type: Behlke HTS 31-06-C) provide the voltage on S15 and S17. The fast switches can change their voltages from one level to another. An independent DC potential is applied to S16. All DC voltages for the different electrodes are provided from a universal multi-channel power supply (CAEN, type: SY5527LC) having four 12-channel high voltage boards for positive voltages (type: AG 538DP, +1.5 kV, 10 mA) and one 12-channel board for negative voltages (type: AG 538DN, -1.5 kV, 10 mA). We developed the electric circuits with a ferrite core-based coil to operate the buncher and ion guide at the required RF voltages [22]. Generally, the miniature buncher and miniature ion guide are operated at RF voltages with an amplitude of  $\leq 35 V_{pp}$ . Since the required

RF voltage is small, two arbitrary function generators (type: Agilent LXI 33522A) are sufficient to drive both required resonance frequencies at nearly 990 kHz.

For proper ion bunching at the trapped segment (S16), the DC potentials of neighbouring segments, S15 and S17, are triggered every measurement cycle as performed in reference[22]. The switching of S17 provides the initial time reference. After the ion bunch drifts through the drift tube, it is transported by the miniature ion guide from the drift tube exit to the PS2.

In the PS2, the ion bunches are transported by another RF ion guide. This ion guide is 327 mm long, and it comprises 21 segments. Each segment is about 15 mm long, and the distance between the opposite rods, which have an 11 mm diameter, is 9.5 mm. The spacing between segments is 0.5 mm. This ion guide's required RF voltage is nearly  $288 V_{pp}$ , generated through an RF amplifier (type: HLA 150). A small DC gradient (15 mV/mm) is applied across the ion guide to transport the ion bunches efficiently.

### C. Cryogenic Drift-tube

The cryogenic drift tube is essentially the heart of the ion mobility spectrometer. It allows ion bunches to drift through the buffer gas under a uniform electric field. The drift tube is a hexagonal tube with an inner diameter of 46 mm, a total external length of 153 mm, and a drift length of approximately 143.5 mm. Two electrically isolated end caps enclose the drift tube. These end caps function as ring electrodes and are sealed from one side by a 1 mm thick plate with a 1.5 mm diameter pinhole at its centre. Thus, it forms a volume isolated from the pressure section, PS1. Figure 2 shows the cross-sectional view of Cryogenic drift cell in Ion mobility mass spectrometer setup. The drift tube consists of 24 stainless steel ring electrodes. These ring electrodes have an inner diameter of 20 mm, an outer diameter of 24 mm, and a width of 5 mm. They are supported by Vitronit ceramic rods that are fixed at the end caps. The ceramic cylindrical spacers maintain a separation of 0.5 mm between the electrodes, which are electrically isolated from the drift tube housing. The electrodes are connected by a series of 500 k $\Omega$  resistors, resulting in a resistance of 11.5 M $\Omega$  between the end caps. The drift tube chamber is externally plated with a thin copper layer (50–100  $\mu$ m thickness) to enhance heat conductance and ensure a homogeneous temperature distribution during cooling and warming phases. It features a gas inlet and outlet, a connection for a pressure gauge (Type: Pfeiffer, CMR 261, part no. PTR 24502), tapered holes for connecting resistive heaters (high-power resistors TCP100U) and temperature sensors (Lake Shore Germanium-CD). The drift tube connects to a free-piston Stirling cryocooler (type: CryoTel-CT, cooling capacity: 11 W, 77K) via four cop-

per strands with a cross-sectional area of 16 mm<sup>2</sup>. The entire drift tube is held to the outer chamber using 12 titanium spokes (M2, DIN 975/DIN 976 Titanium Grade 2). Additional details of a similar drift tube configuration can be found in ref [23],[22], [24]. Although the drift tube has a cryogenic temperature facility, it operates only with helium and only at room temperature (298 K).

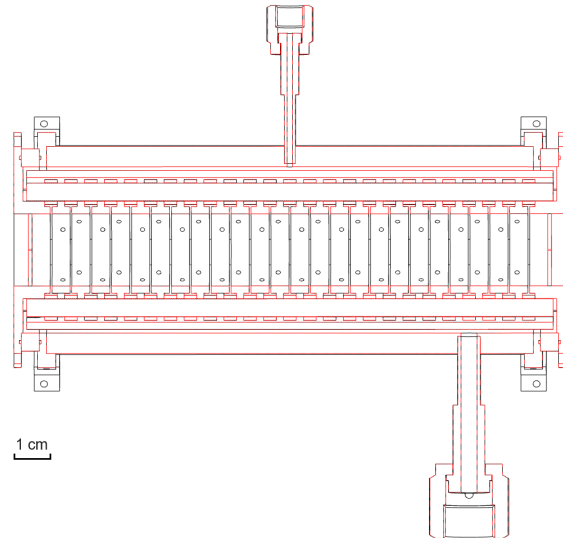


FIG. 2: Cross-sectional view of Cryogenic drift cell in Ion mobility mass spectrometer setup.

### D. Quadrupole Mass Filter and detector

Mass separation is achieved through a quadrupole mass filter (QMF) (type: Balzers QMG 311). This mass filter can be remotely controlled to select an ion mass-to-charge ratio of up to 300 u/e with a mass resolution of up to 0.2 u/e. The data acquisition system controls the QMF operation via an analog interface. After the QMF, a 90-degree deflector and electrostatic lenses are installed to deflect and focus the ions into a channeltron detector (Sjuts, CEM, KBL 15RS). A user-friendly data acquisition module with a LabVIEW interface was developed. Various parameters, such as voltages on different electrodes, mass resolution, etc., were remotely controlled, and the measured data was recorded.

## III. RESULTS AND DISCUSSION

### A. Optimization of miniature RF ion buncher

We used laser ablated Lu<sup>+</sup> as a test sample to characterize the developed ion mobility spectrometer. Fig. 3 displays the mass scan obtained from the QMF with a



resolution of 0.2 u/e, clearly showing the two Lu isotopes ( $\text{Lu}^{175}$  and  $\text{Lu}^{176}$ ) and their corresponding monoxides. During the experiments, the QMF was typically set at a high resolution of 0.5 u/e to be able to resolve one atomic mass unit.

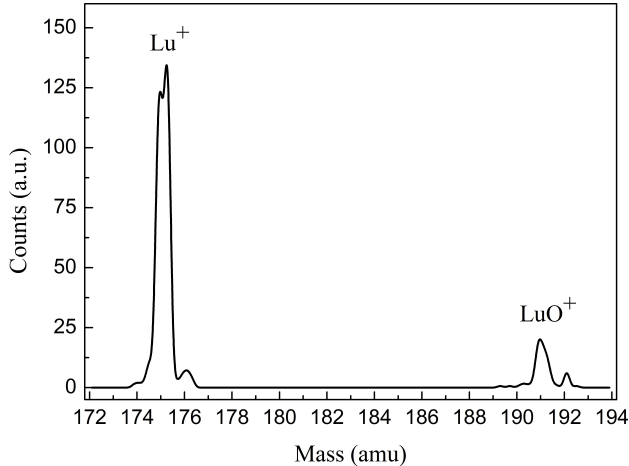


FIG. 3: Mass spectra obtained by laser ablation from a metallic thin foil of lutetium.

To optimize the RF voltage applied to a miniature ion buncher, we measured counts at different amplitudes of the RF voltages, as illustrated in Fig. 4. The RF structure can be seen as a high pass filter with a minimum cut-off mass. We found that approximately 35 V peak-to-peak ( $V_{pp}$ ) of RF voltage is optimum for efficient ion transport through the RF structure within the mass range of lanthanide cations.

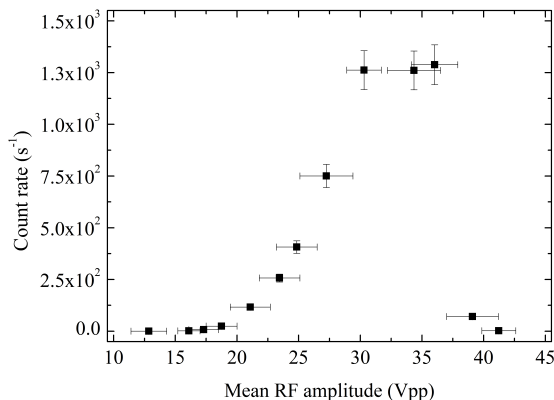


FIG. 4: Optimization of count rate with amplitude of RF voltages applied to the miniature RF buncher.

To initiate the ion bunching operation, we first trap the ions by creating a potential well at the position of the S16 electrode. This is achieved by applying a +10 V higher potential on the last electrode, S17, compared to

the S16 electrode, whereas the voltage on S16 is one volt lower than the previous electrode, S15. Consequently, the ions accumulate in the potential well and cool down at the position of the S16 electrode. Following the laser ablation pulse at a predetermined time delay of 10 milliseconds, the potential at the S15 electrode is increased by +25 V from its set value to kick the ion bunch forward, and sequentially, the potential at the S17 electrode is decreased to allow the ion bunch to be injected into the drift tube. This latter action sets the time reference  $t = 0$  for the ions' arrival time distribution. It was observed that the kicking potential on electrode S15 needs to be increased at higher drift tube pressures as the ions have to be injected into the drift tube, counter-propagating the gas stream formed at the tube entrance. A similar buncher operation has been reported in former work [22]. A typical arrival time distribution of  $\text{Lu}^+$  ions in bunching mode operation is depicted in Fig. 5, along with the distribution in transmission mode. It is observed that the full width at half maximum (FWHM) decreases from 4 ms in transmission mode to 60  $\mu\text{s}$  in bunching mode.

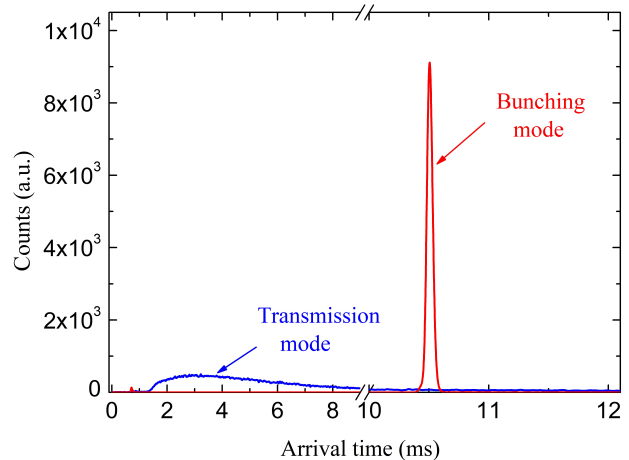


FIG. 5: Arrival time distribution of  $\text{Lu}^+$  ions in transmission and bunching operation modes at a helium pressure of 8 mbar in the drift tube and  $8 \cdot 10^{-2}$  mbar in section PS2. In bunching mode, a delay time of 10 ms was implemented to cool down and bunch ions after ablation. The initial tiny peak indicates the arrival of a small fraction of the initial ion bunch with high  $K \cdot E$  from the source.

## B. Chromatography performance of drift tube

To evaluate the performance of the drift tube, we measured the mean arrival time of ions bunch at different He pressures, ranging from 1.5 mbar to 8 mbar and reduced electric fields spanning 1 to 20 Td. The reduced electric field ( $E/n_0$ ) represents the ratio of the electric field ( $E$ ) applied across the drift tube to the neutral gas number density ( $n_0$ ). It is expressed in Td (Townsend units),

where 1 Td equals  $1 \cdot 10^{-17}$  Vcm<sup>2</sup>. It is observed that the mean-time is nearly the same for a fixed reduced field at buffer gas pressures exceeding 2 mbar, which implies a steady state condition for ion drift. For a fixed buffer gas pressure, it follows equation 1 and scales with the electric field.

Furthermore, we analyzed the FWHM of mean arrival times under different reduced electric fields and drift tube pressures. Fig. 6 illustrates the relative width ( $\Delta t/t$ ) of the arrival time distribution vs. the reduced electric field for different gas pressures. As it mentioned above, the mean arrival time remains unchanged at different pressures for a given reduced field. However, longitudinal diffusion decreases with increasing drift tube pressure due to enhanced collision rates. Consequently, the relative width ( $\Delta t/t$ ) decreases with increasing He pressure, reaching a minimum of approximately 6% at a reduced electric field of 4 Td which should enable the differentiation of ion mobilities with this relative difference.

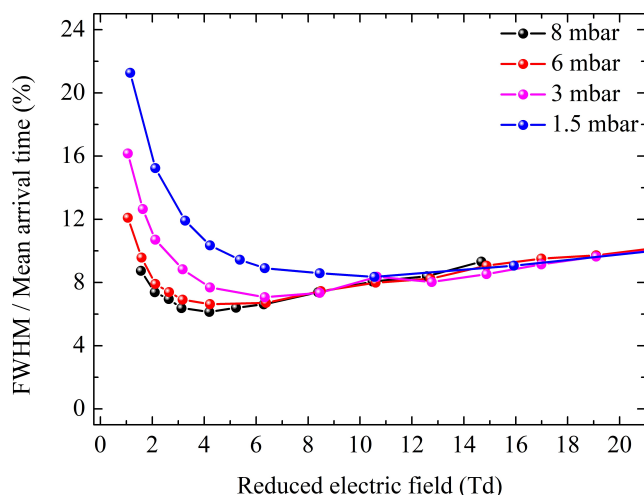


FIG. 6: Time resolution of developed ion mobility mass spectrometer with the reduced electric field for different He pressure in the drift tube.

### C. Electronic state chromatography and measurement of low field mobility

Electronic state chromatography (ESC) is a well-studied effect and has been reported for many transition metal ions drifting in helium [17]. The effect becomes most pronounced and relatively easy to observe when ions with completely different electronic configurations are present. In the case of Lu<sup>+</sup>, the ESC effect was first time reported by our group[22]. Fig. 7 shows the measured arrival time distribution of Lu<sup>+</sup> with 8 mbar He pressure and 5 Td reduced field at the laser power of 9 mW and 16 mW. Two distinct peaks have been observed. The slower peak corresponds to the arrival dis-

tribution of ground state (6s<sup>2</sup>) ions, and the first peak is the same as metastable state (5d<sup>1</sup>6s<sup>1</sup>)ions as the population of metastable ions is expected to be higher at the higher laser power. It suggests the Lu<sup>+</sup> in the ground state (with two s electrons) interacts more strongly with helium than the metastable state, which possesses only one s electron.

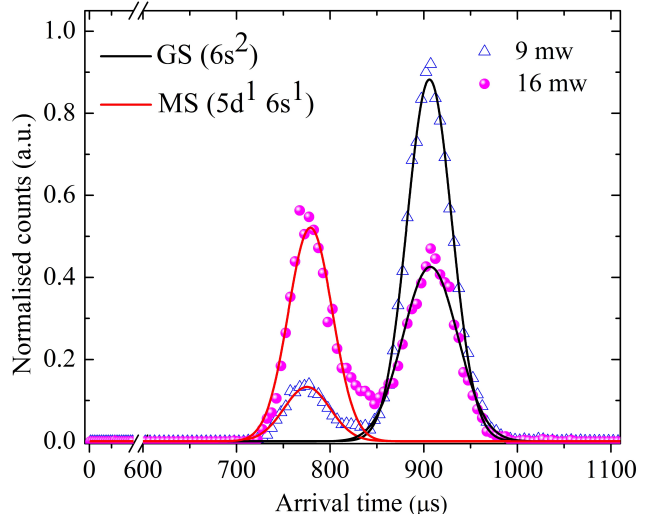


FIG. 7: Arrival time distributions of Lu<sup>+</sup> ablated at 5 mW (○), 9 mW (Δ), (●) laser powers and 16 mW used for ablation of Lu<sup>+</sup> after their drift in helium at pressure 8 mbar under the influence of reduced electric field 5 Td. Solid lines indicate the Gaussian fit to the data.

The mean arrival time ( $t_{ATD}$ ) of an ion bunch consists of two components: the drift time ( $t_d$ ), which is the time the ions spent within the drift tube and an offset time of flight ( $t_{offset}$ ), which the ions spent outside of the drift tube. It is expressed as:

$$t_{ATD} = \left( \frac{L^2 T_0}{K_0 P_0 T} \right) \left( \frac{P}{V} \right) + t_{offset}. \quad (4)$$

Here,  $L$  is the drift length, and  $V$  is the voltage difference across the length. The measured time distribution is fitted with two Gaussian functions to extract the mean arrival times. Figure 8 presents the plot of such estimated mean arrival times at different values of  $P/V$ . It gives a linear plot from which  $K_0$  is deduced as per equation no 4. In order to extract the low-field reduced mobility, we consider only the data points taken at reduced fields less than 5 Td. In general, the measured values of reduced mobilities have an uncertainty of 2%, mainly arising from buffer gas pressure fluctuations of 0.1 mbar. The estimated low field reduced mobilities of Lu<sup>+</sup> are 16.6 (0.2) cm<sup>2</sup>/V s and 19.7 (0.3) cm<sup>2</sup>/V s for the ground and metastable states, respectively. Table I shows the measured values along with the literature values. These values are the mean of five measurements,

with standard deviations in parentheses. The measured value of the ground state agrees well with the reported value measured by Manard *et.al.* [25] and the theoretically calculated value from *abinitio* calculations [26]. The measured low field reduced mobility of metastable  $\text{Lu}^+$  is a first-time addition to the literature. It matches the calculated value of  $19.5 \text{ cm}^2/\text{V s}$  from MRCI calculations [26]. The estimated difference in the ion mobility is 15.7%, and the developed ion mobility spectrometer well resolves the arrival time for the different states. The state-specific zero field diffusion coefficient ( $n_0D$ ) of  $\text{Lu}^+$  in the ground state and metastable state is also estimated from Einstein relation [12] and listed in table I.

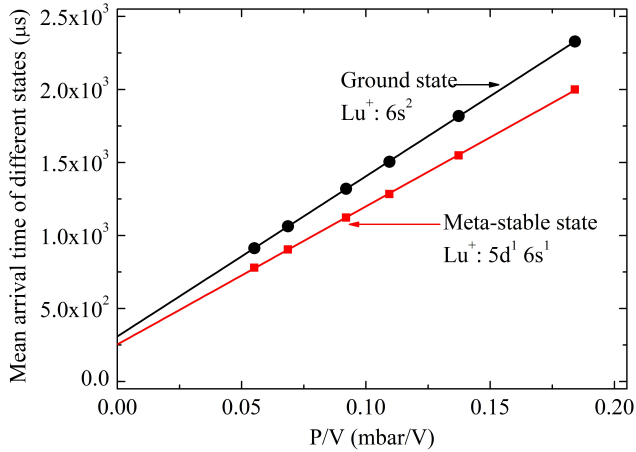


FIG. 8: Arrival time of  $\text{Lu}^+$  ions for both ground and meta-stable states with different pressure to the applied potential across the drift tube. Solid lines are linear fittings of the data points for separate states.

TABLE I: Estimated reduced ion mobilities and corresponding diffusion coefficients of  $\text{Lu}^+$  for its ground state and meta-stable state.

$K_0(\text{cm}^2/\text{V s})$		$n_0D (10^{19}/\text{cm s})$		
GS	MS	GS	MS	
16.6 (0.2)	19.7 (0.3)	1.05	1.30	This work
16.8 (0.04)	—	—	—	Manard <i>et al.</i> [25]
16.5	19.5	1.07	1.30	Ramanantoanina <i>et al.</i> [26]
16.6	20.6	1.07	1.33	Laatiaoui <i>et al.</i> [19]

Figure 9 shows the variation of reduced mobility with the reduced field up to 20 Td, along with theoretically estimated values [19], [26]. It has been observed that the reduced ion mobility of  $\text{Lu}^+$  remains nearly constant at lower reduced field values, and it decreases gradually with increasing reduced fields. This is because as the reduced field increases, the ion kinetic energy increases which leads to an increase in the effective ion temperature beyond that given by the surrounding He buffer gas. It

increases collision cross-section, thereby decreasing ions' reduced mobility according to equation 3. The measured value of ground state mobility of  $\text{Lu}^+$  at lower reduced fields equally matches the theory predictions based on scalar relativistic and MRCI interaction potentials. In the case of metastable state mobility, a slight deviation is noticed between the measured values and the theory estimations, which we trace back to the degree of accuracy applied for the prediction of the ion-atom interaction potential. These measurements serve as valuable benchmarks for modern *abinitio* calculations.

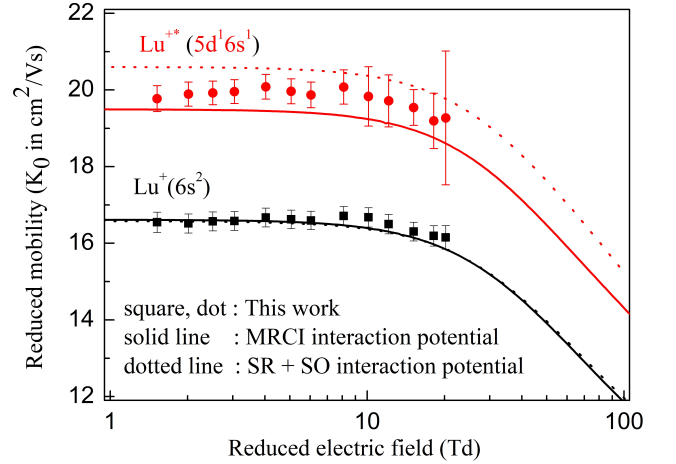


FIG. 9: Comparison between measured reduced ion mobility of  $\text{Lu}^+$  for ground state and metastable state with theory at different reduced electric fields.

#### D. Deactivation of metastable level population

From the two Gaussian function fits, we estimated the area under the Gaussian curve for the two observed peaks for  $\text{Lu}^+$ . It gives the population of ions in their ground state and metastable states. Figure 10 shows the normalized population of the metastable level as a function of the reduced electric field. It is observed that the deactivation of the metastable level population occurs due to collisional quenching. At a higher reduced electric field, the ions gain more kinetic energy between collisions. When the ions with higher K.E. collide with He or another ions, it increases the rate of deactivation for the metastable level population. This phenomenon could be explained from the interaction potential curve of  $\text{Lu}^+$  with ground state and metastable state with neutral Helium [27]. There is a cross over of two surface of interaction potential for metastable state and ground state at a smaller inter-nuclear distance. It allows a mixing of two states and gives a quenching pathways at the higher ions' kinetic energy. At a fixed reduced field, the metastable level population slowly increases with the He pressure, as shown in the inset of figure 9. As the He pressure inside the drift tube increases, the number of collisions be-

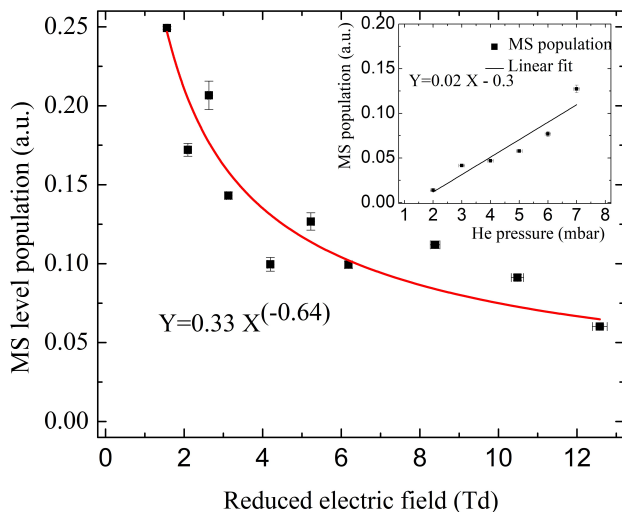


FIG. 10: Deactivation of  $\text{Lu}^+$  meta-stable level population due to collision quenching with the reduced electric field. The Solid line is the best fit for the data. (inset), variation of the metastable level population with the drift tube pressure at a fixed reduced field (6 Td)

tween  $\text{Lu}^+$  and He increases. It results in less diffusion of the injected ion cloud in the transverse direction and increases the overall transmission of  $\text{Lu}^+$  through the drift tube. Since the difference in ion mobility allows for different diffusion coefficients, there is a different expansion of injected ion cloud for the metastable and ground-state. With less mobility, the ground state takes longer to travel through the drift tube. This leads to a larger ground-state ion cloud compared to the metastable state. It is expected more loss of ground state ions compared to that of metastable ions and it indirectly increases the normalized population of the metastable state. The collision quenching rate is nearly a linear function of pressure at a fixed reduced field. Moreover, the deactivation of the higher excited level depends on the reduced electric field and is influenced by the energy level gap between the

ground and metastable states.

#### IV. SUMMARY AND OUTLOOK

A new cryogenic ion mobility spectrometer apparatus has been developed and thoroughly characterized. The bunching operation with a miniature RF ion buncher has been optimized, and the performance of the cryogenic drift tube has been evaluated. Electronic state chromatography for  $\text{Lu}^+$  ions has been demonstrated by measuring their low-field reduced ion mobility in both ground state and metastable state. The measured values show good agreement with literature values and theoretical predictions. Additionally, the variation in reduced mobility of  $\text{Lu}^+$  with the reduced electric field for both the ground state and metastable state, and the deactivation of the metastable population due to collisional quenching, have been examined.

The next steps include measuring the low-field reduced mobility of different lanthanide cations in their ground state and metastable states if possible, with different buffer gases such as helium and argon, before extending such measurements to the actinides. Since ion mobility is sensitive to electronic configuration, we hope this research will deepen our understanding of the interplay between transport properties and relativistic effects in the region of the heaviest elements.

#### V. ACKNOWLEDGEMENTS

This project has received funding from the Deutsche Forschungs Gemeinschaft (DFG), German Research Foundation (Project No. 426500921) and the European Research Council (ERC) under the European Union's Horizon 2020 research and innovation programme (grant agreement No. 819957).

- [1] M. Schädel, "Chemistry of the superheavy elements," *Philosophical Transactions of the Royal Society A: Mathematical, Physical and Engineering Sciences*, vol. 373, no. 2037, p. 20140191, 2015.
- [2] P. Pyykkö, "Relativistic effects in chemistry: more common than you thought," *Annual review of physical chemistry*, vol. 63, pp. 45–64, 2012.
- [3] H. Tatewaki, S. Yamamoto, and Y. Hatano, "Relativistic effects in the electronic structure of atoms," *ACS omega*, vol. 2, no. 9, pp. 6072–6080, 2017.
- [4] P. Schwerdtfeger, L. F. Pašteka, A. Punnett, and P. O. Bowman, "Relativistic and quantum electrodynamic effects in superheavy elements," *Nuclear Physics A*, vol. 944, pp. 551–577, 2015.
- [5] A. Das, U. Das, R. Das, and A. K. Das, "Relativistic ef-

- fects on the chemistry of heavier elements: why not given proper importance in chemistry education at the undergraduate and postgraduate level?," *Chemistry Teacher International*, vol. 5, no. 4, pp. 365–378, 2023.
- [6] B. G. Wybourne and L. Smentek, "Relativistic effects in lanthanides and actinides," *Journal of alloys and compounds*, vol. 341, no. 1-2, pp. 71–75, 2002.
- [7] V. Pershina, "Relativistic effects on the electronic structure of the heaviest elements. is the periodic table endless?," *Comptes Rendus. Chimie*, vol. 23, no. 3, pp. 255–265, 2020.
- [8] V. Gabelica, "Ion Mobility–Mass Spectrometry: an Overview," in *Ion Mobility – Mass Spectrometry: Fundamentals and Applications*, The Royal Society of Chemistry, 11 2021.

- [9] C. L. Wilkins and S. Trimpin, *Ion mobility spectrometry-mass spectrometry: theory and applications*. CRC press, 2010.
- [10] E. Christofi and P. Barran, “Ion mobility mass spectrometry (im-ms) for structural biology: insights gained by measuring mass, charge, and collision cross section,” *Chemical Reviews*, vol. 123, no. 6, pp. 2902–2949, 2023.
- [11] L. Viehland, *Gaseous Ion Mobility, Diffusion, and Reaction*. Cham, Switzerland: Springer Nature AG, 2018.
- [12] E. Mason and E. McDaniel, *Transport Properties of Ions in Gases*. New York: John Wiley and Sons, 1988.
- [13] H. Backe, W. Lauth, M. Block, and M. Laatiaoui, “Prospects for laser spectroscopy, ion chemistry and mobility measurements of superheavy elements in buffer-gas traps,” *Nuclear Physics A*, vol. 944, pp. 492–517, 2015.
- [14] M. Laatiaoui, H. Backe, D. Habs, P. Kunz, W. Lauth, and M. Sewtz, “Low-field mobilities of rare-earth metals,” *The European Physical Journal D*, vol. 66, p. 232, 2012.
- [15] G. Visentin, M. Laatiaoui, L. A. Viehland, and A. A. Buchachenko, “Mobility of the singly-charged lanthanide and actinide cations: Trends and perspectives,” *Frontiers in Chemistry*, vol. 8, p. 438, 2020.
- [16] M. J. Manard and P. R. Kemper, “An experimental investigation into the reduced mobilities of lanthanide cations using high-resolution ion mobility mass spectrometry,” *International Journal of Mass Spectrometry*, vol. 423, pp. 54–58, 2017.
- [17] P. Kemper and M. Bowers, “Electronic-state chromatography: application to first-row transition-metal ions,” *J. Phys. Chem.*, vol. 95, pp. 5134–5146, 1991.
- [18] Y. Ibrahim *et al.*, “Ion Mobility of Ground and Excited States of Laser-Generated Transition Metal Cations,” *J. Phys. Chem. A*, vol. 112, p. 1112, 2008.
- [19] M. Laatiaoui, A. A. Buchachenko, and L. A. Viehland, “Laser resonance chromatography of superheavy elements,” *Physical Review Letters*, vol. 125, no. 2, p. 023002, 2020.
- [20] W. Paul, “Electromagnetic traps for charged and neutral particles,” *Reviews of modern physics*, vol. 62, no. 3, p. 531, 1990.
- [21] M. Drewsen and A. Brøner, “Harmonic linear paul trap: Stability diagram and effective potentials,” *Physical Review A*, vol. 62, no. 4, p. 045401, 2000.
- [22] E. Kim, B. Jana, A. Arya, M. Block, S. Raeder, H. Ramanantoanina, E. Rickert, E. R. Romero, and M. Laatiaoui, “Laser resonance chromatography: First commissioning results and future prospects,” 2024.
- [23] E. Romero Romero, M. Block, B. Jana, E. Kim, S. Nothhelfer, S. Raeder, H. Ramanantoanina, E. Rickert, J. Schneider, P. Sikora, and M. Laatiaoui, “A progress report on laser resonance chromatography,” *Atoms*, vol. 10, no. 3, 2022.
- [24] E. Rickert, *Laser spectroscopy of fermium isotopes and development of an actinide ion mobility spectrometer*. PhD thesis, Mainz, 2023.
- [25] M. Manard and P. Kemper, “Reduced mobilities of lanthanide cations measured using high-resolution ion mobility mass spectrometry with comparisons between experiment and theory,” *Int. J. Mass Spectrom.*, vol. 412, p. 14, 2017.
- [26] H. Ramanantoanina *et al.*, “State-specific ion mobilities of  $\text{Lr}^+$  ( $Z = 103$ ) in helium,” *Physical Review A*, vol. 108, p. 012802, 2023.
- [27] M. Laatiaoui, A. A. Buchachenko, and L. A. Viehland, “Exploiting transport properties for the detection of optical pumping in heavy ions,” *Physical Review A*, vol. 102, p. 013106, jul 2020.